nature chemistry

ARTICLES

PUBLISHED ONLINE: 27 JUNE 2010 | DOI: 10.1038/NCHEM.719

Etching and narrowing of graphene from the edges

Xinran Wang and Hongjie Dai*

Large-scale graphene electronics requires lithographic patterning of narrow graphene nanoribbons for device integration. However, conventional lithography can only reliably pattern ~20-nm-wide GNR arrays limited by lithography resolution, while sub-5-nm GNRs are desirable for high on/off ratio field-effect transistors at room temperature. Here, we devised a gas phase chemical approach to etch graphene from the edges without damaging its basal plane. The reaction involved high temperature oxidation of graphene in a slightly reducing environment in the presence of ammonia to afford controlled etch rate (≲1 nm min^{-1}). We fabricated ~20–30-nm-wide graphene nanoribbon arrays lithographically, and used the gas phase etching chemistry to narrow the ribbons down to <10 nm. For the first time, a high on/off ratio up to ~10^4 was achieved at room temperature for field-effect transistors built with sub-5-nm-wide graphene nanoribbon semiconductors derived from lithographic patterning and narrowing. Our controlled etching method opens up a chemical way to control the size of various graphene nano-structures beyond the capability of top-down lithography.

Graphene has attracted much attention as a novel two-dimensional system with great potential in future electronics developments[1,2]. Narrow graphene nanoribbons (GNRs) have been used as semiconducting wires in field-effect transistors (FETs) that have high on/off ratios at room temperature[3–9]. Of the various methods used to produce narrow GNRs, including chemical sonication[3] and unzipping of carbon nanotubes[5,10], top-down lithographic patterning of a large pristine graphene sheet into GNRs is appealing for large-scale device integration[2]. To date, patterning methods have only produced arrays of GNRs with widths down to ~20 nm (except for short, narrow constrictions[9]) because of the limits of lithography resolution[7,8], but GNRs narrower than ~5 nm with sufficiently large bandgaps are needed for room-temperature FET operation[3–6,11–13]. Here, we demonstrate a gas-phase chemical approach to etching graphene from the edges without damaging its basal plane. The reaction involves high-temperature oxidation of the graphene in a slightly reducing environment, resulting in controlled (≲1 nm min^{-1}) etching. We fabricated ~20–30-nm-wide GNR arrays by electron-beam lithography, and subsequently narrowed the GNRs using the gas-phase etching process. When GNRs narrowed to ≲5 nm were used in GNR-FETs, bandgap opening related to quantum confinement was clearly observed. For the first time, an on/off ratio up to ~1×10^4 was achieved at room temperature in devices with ≲5-nm-wide GNR channels derived from lithographic patterning. Parallel arrays of ~8-nm-wide GNRs were used to produce FETs with an on/off ratio ~50 and with 'on' currents far exceeding those of single-ribbon devices. Controlled chemical etching could therefore play an important role in tailoring the dimensions of graphene for large-scale device integration.

To devise a gas-phase chemistry process for etching and narrowing graphene from the edges without creating defects in the basal plane, we investigated chemical etching of few-layer (≲3 layers) mechanically exfoliated graphene on a 300-nm SiO_2/Si substrate under various oxidation conditions at high temperatures (Fig. 1 and Supplementary Figs S1,S2; see Methods for experimental details). We varied the partial pressure of O_2 and introduced Ar, H_2 or NH_3 as a dilution gas or to provide a reducing environment. We found that etching of the graphene was highly dependent on the gas mixture and reaction temperature, as well as on the number of layers of graphene (Supplementary Table S1). At 750 °C, ~100 mtorr of O_2 diluted by ~1 torr of Ar or H_2 gave an etch rate of ~3–5 nm min^{-1} (~6–7 nm min^{-1}) for single- (double-) layer graphene (Supplementary Fig. S1). Interestingly, when using ~100 mtorr O_2 with ~1 torr 10% NH_3 in Ar as additive, we observed a considerably slower etching rate of ~2–2.5 nm min^{-1} (~4 nm min^{-1}) for single- (double-) layer graphene (Supplementary Fig. S2). We then reduced the O_2 partial pressure to ~25 mtorr with a view to achieving slower etching. Under ~25 mtorr O_2 and ~1 torr H_2, the etching rate at 800 °C was ~3−3.5 nm min^{-1} (~3.8−5 nm min^{-1}) for single- (double-) layer graphene (Supplementary Fig. S1). By introducing NH_3 into the system, we found that the etching rate was further lowered to less than ~1 nm min^{-1} under ~25 mtorr of O_2 in ~1 torr of 10% NH_3 in Ar (Fig. 1, Supplementary Fig. S1 and Table S1). A slow etching rate is highly desirable for the controlled etching and narrowing of graphene and GNRs down to the ≲5 nm regime.

We observed that graphene etching occurred predominantly at the edges and proceeded inwards isotropically (Fig. 1, Supplementary Figs S1,S2). As a result of the presence of bond disorders and functional groups at the edges of the graphene, the chemical reactivity of the edge carbon atoms was higher than the perfectly bonded sp^2 carbon atoms in the basal plane[14]. Consequently, the graphene sheets were etched uniformly from the edges under controlled oxidation conditions. Holes or trenches were occasionally observed to have formed in the graphene due to etching that had initiated at point defects or line defects, respectively, within the graphene plane (Fig. 1d−f, Supplementary Fig. S1)[14–16]. Certain line defects were visible under atomic force microscopy (AFM), including wrinkles (Fig. 1d), although not all defects were observed by AFM (Supplementary Fig. S1a–b,d–e). Importantly, Raman spectroscopic mapping and imaging revealed that etching from the edges did not damage the basal plane of the pristine graphene, as indicated by the absence of the defect-related Raman band (D band) in the plane of the graphene sheets following etching (for example, Fig. 1g–i, Supplementary Fig. S2c,d). We observed redshifts of the Raman G band of graphene after etching in both O_2/NH_3 (Fig. 1i) and O_2/Ar conditions, which could not be fully explained but could be due to strain in the graphene sheets, indicated by the formation of the wrinkles sometimes observed following the high-temperature reaction process (Fig. 1e, Supplementary Fig. S1b,e)[17,18].

Department of Chemistry and Laboratory for Advanced Materials, Stanford University, Stanford, California 94305, USA. *e-mail: hdai@stanford.edu

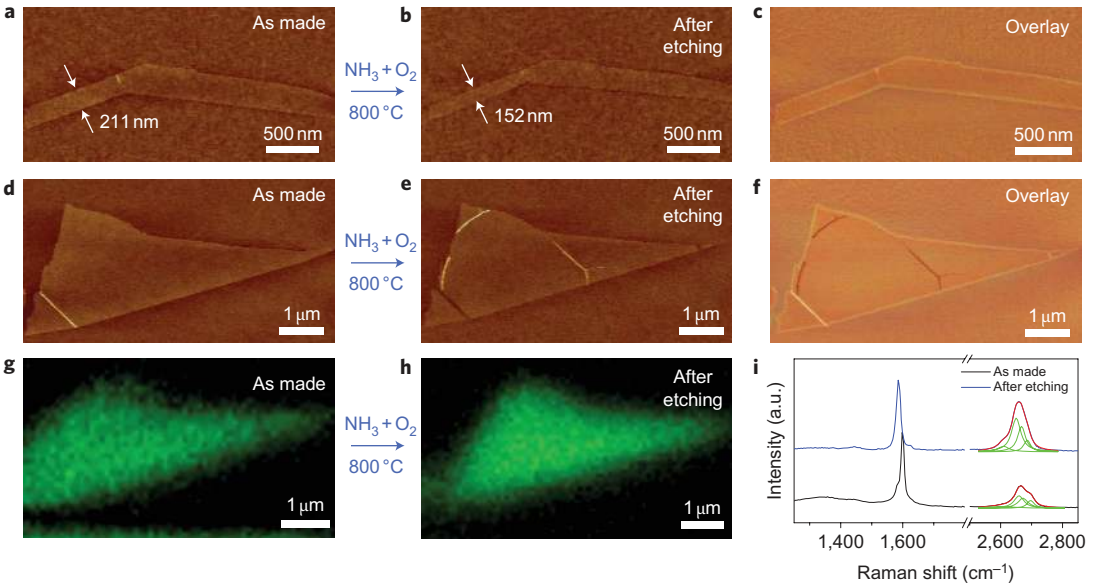

Figure 1 | Gas-phase chemical etching and narrowing of graphene sheets. The etching conditions were ~25 mtorr O_2 in the presence of ~1 torr 10% NH_3 in Ar at 800 °C for 1 h. **a**,**b**, Graphene sheet imaged by AFM: as-made (**a**) and after etching (**b**). **c**, Overlay images before (yellow) and after (red) etching, with uniform etching from the edges observed at an etching rate of ~0.5 nm min^{-1}. **d**–**f**, Another set of graphene sheet etching data. A wrinkle with high strain (bright strip) on the as-made graphene was etched away to form a trench. Etching rate, ~0.8 nm min^{-1}. Note that new wrinkles (bright lines in **e**) were observed after the reaction, probably caused by thermal effects. **g**,**h**, Raman G band mapping of the graphene sheet in **d** and **e** before (**g**) and after (**h**) etching. **i**, Averaged Raman spectra from the graphene plane in **g** and **h**. The 2D band can be fit into 4 Lorentzians for both as-made and after-etching cases, indicating two-layer graphene both before and after etching[21]. No obvious D band is observed after etching in the plane of the graphene.

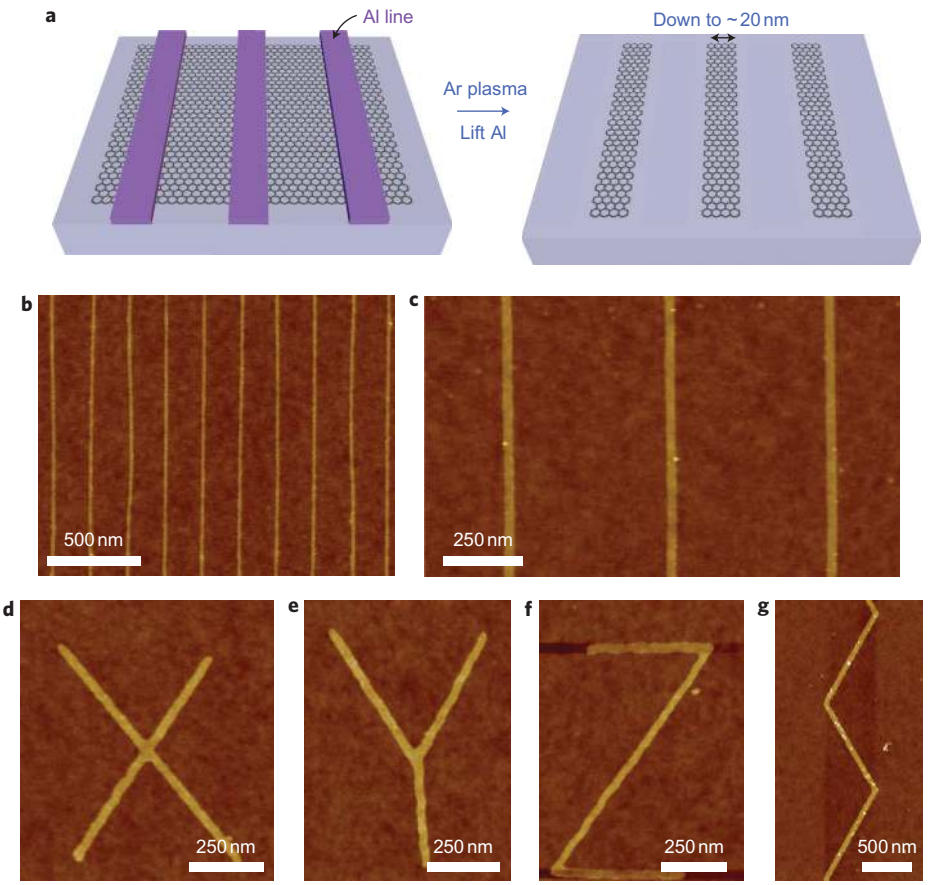

Figure 2 | Lithographically patterned GNR arrays and junctions. a, Schematics of the fabrications process. **b**, AFM image of a $w \approx 20$ nm GNR array at ~200 nm pitch. **c**, High-resolution AFM image of a $w \approx 22$ nm GNR array at ~500 nm pitch. **d**–**g**, AFM images of various GNR structures including alphabetic characters and zigzag junctions.

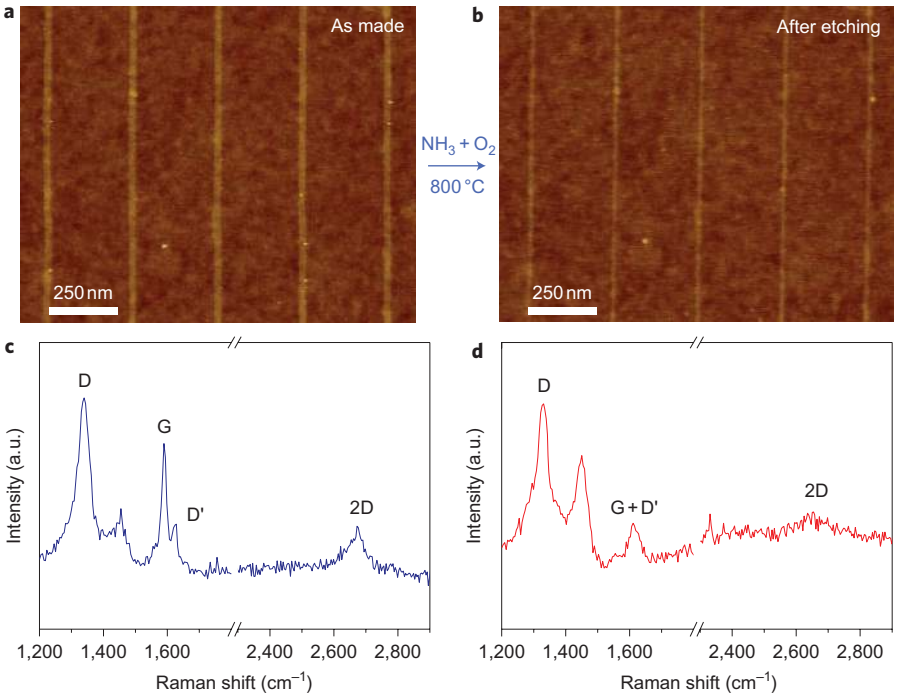

Figure 3 | Gas-phase chemical narrowing of GNRs. a,**b**, AFM images of a GNR array: as-made (**a**) and after chemical narrowing (**b**). The narrowing conditions were ~25 mtorr O_2 in the presence of ~1 torr 10% NH_3 in Ar at 800 °C for 10 min. The GNRs were narrowed uniformly from ~20 to ~8 nm with no obvious breaks. Etching rate, ~0.6 nm min^{-1}. **c**,**d**, Averaged Raman spectra of the GNR arrays from **a** and **b**.

Our graphene etching process involves O_2 oxidation of graphene into CO or CO_2. During etching, O_2 molecules exothermally dissociate and form bonds with dangling carbon atoms at defect sites and edges[15,16]. The slower etching rate observed under the NH_3 environment was attributed to *in situ* NH_3 reduction of oxygen groups formed during graphene oxidation. Our recent work on the reduction of graphene oxide suggests that NH_3 is more effective than H_2 in reducing oxygen groups in graphene oxide[19], and the NH_3 reduction effect could impede the oxidation of graphene when mixed with oxygen. It was also interesting that, under the same reaction conditions, thicker graphene sheets were etched more quickly than thinner ones (Supplementary Table S1, Fig. S2), a finding that is similar to earlier observations made for thick graphite[15,16]. This also could not be fully explained, but could be due to the synergistic effects of oxygen groups at the edges of adjacent layers leading to self-catalysed etching at the edges of multilayer graphene[16]. As a control, we heated graphene in pure ammonia, and did not observe any etching effects (Supplementary Fig. S3a).

We next fabricated GNR arrays by lithographic patterning, and used our gas-phase reaction to narrow the as-made ribbons to a width of several nanometres. GNR arrays were fabricated by electron-beam lithography and Ar plasma etching of exfoliated graphene on a 300-nm SiO_2/Si substrate (Fig. 2a; see Methods for details of the fabrication process). Rather than using the electron-beam resist as the etch mask[7–9], we instead used thin (~6.5 nm) Al lines (defined by a single-pixel electron beam) (Fig. 2a; see also Supplementary Information). The widths of the GNRs were measured by AFM with finite tip size deconvolution[3]. The as-patterned GNRs had widths as narrow as ~20 nm, with a mean edge roughness $\delta w = (w_{max} - w_{min})/2 \lesssim 5$ nm (Fig. 2b–g). The edge roughness was caused by random fluctuating factors in the lithography and plasma etching processes[6–9]. Lithographic patterning using Al as an etch mask is versatile, enabling graphene to be patterned into various structures with high reproducibility and consistency. For example, we easily fabricated alphabetic characters and junctions using GNRs with $w \approx 20$ nm (Fig. 2d–g); these could form interesting structures with which to study electron transport along the various crystallographic directions of graphene[20,21].

To create GNR-FETs with a high I_{on}/I_{off} ratio at room temperature, GNRs with $w \lesssim 5$ nm and sufficiently large bandgap ($E_g \gg k_B T \approx 26$ meV) were required[3–6,11,13]. We narrowed down the as-made $w \approx 20$ nm GNRs using the 0.5–1 nm min^{-1} etching condition (25 mtorr O_2 in 1 torr NH_3/Ar at 800 °C). (It was found to be difficult to narrow the GNRs with good width control in several control experiments using other conditions; Supplementary Fig. S3.) We succeeded in narrowing the GNRs uniformly from ~20 to ~8 nm without obvious breaks along the ribbons (Fig. 3a,b). However, further narrowing generally resulted in breaks due to edge roughness and width variations in the as-patterned GNRs. By over-etching, we obtained ribbons with $w \lesssim 5$ nm, with most GNRs evolving into discontinuous segments down to less than 5 nm in width. Some of the segments were sufficiently long to be useful for integration into FET devices for electrical measurements (Fig. 4d). Edge roughness in as-made GNRs created by lithographic patterning is currently a limiting factor in producing long, uniform ultra-narrow GNRs over large areas.

We carried out Raman spectroscopic measurements on the as-made and narrowed GNRs (Fig. 3c,d). For as-made GNRs with $w \approx 20$ nm, several pronounced peaks were observed, including a D band (~1,340 cm^{-1}), G band (~1,590 cm^{-1}), D′ band (~1,620 cm^{-1}) and 2D band (~2,670 cm^{-1}) (Fig. 3c). The intensity ratio between the D and G bands, I_D/I_G, was ~1−2. The presence of defect-related D and D′ bands was attributed to the edges of GNRs, because no D band was observed in the parent graphene sheet[5,22]. For a GNR with $w \approx 20$ nm, ~1% of the carbon atoms are at the edges, resulting in D and D′ bands as expected[22]. We observed lower I_D/I_G ratios in wider GNRs (see Supplementary Information; Fig. S7), consistent with reduced edge effects. After narrowing to less than ~10 nm, the intensity of the G and 2D bands of the graphene reduced, the I_D/I_G ratio increased, and the G and D′ peaks were broadened to form a single and up-shifted G peak (Fig. 3d)[22]. These changes in the Raman spectra were a

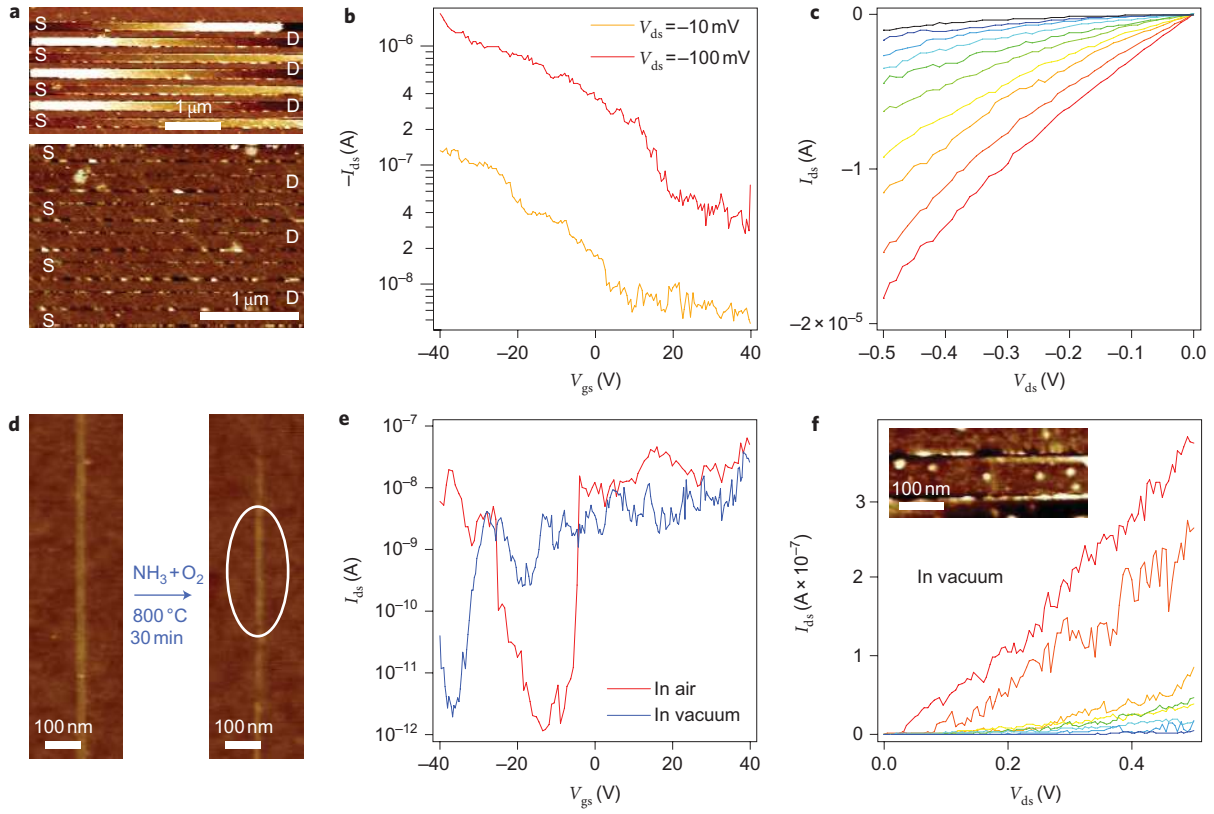

Figure 4 | FETs from lithographically patterned and chemically narrowed GNRs and parallel GNR arrays. a, AFM images of a $w \approx 8$ nm GNR-array FET (top panel, the same array as in Fig. 3b) with interdigitized electrodes used to contact ~40 GNRs in parallel (channel length, ~160 nm). Bottom panel, enlarged image of the device. Source (S) and drain (D) contacts are marked on all images. **b**, Room-temperature $I_{ds}-V_{gs}$ characteristics of the GNR-array FET in **a**, probed in air. The I_{on}/I_{off} ratio is ~50. **c**, $I_{ds}-V_{ds}$ characteristics of the same device in **a**, probed in air. From top to bottom, $V_{gs} = -40$ to 50 V in steps of 10 V. **d**, AFM images of as-made and narrowed GNRs with breaks along the ribbon. The highlighted part is less than 5 nm in width, and was used to make a GNR-FET. **e**, Room-temperature $I_{ds}-V_{gs}$ characteristics of the GNR-FET fabricated from the GNR in **d**. The device demonstrated an I_{on}/I_{off} ratio greater than 10^4 when probed in air and in vacuum. $V_{ds} = 10$ mV for both curves. **f**, $I_{ds}-V_{ds}$ characteristics for the device in **e**, but probed in vacuum. From top to bottom, $V_{gs} = 40$ to −30 V in −10 V steps. Inset: AFM image of the GNR-FET.

result of a higher percentage of the atoms being edge atoms in narrowed GNRs. The I_D/I_G ratios of our narrowed GNRs were larger than similar-width GNRs derived chemically[4], suggesting a higher degree of edge roughness and disorder in the former.

We fabricated electrical devices with as-made and narrowed GNRs with Pd source and drain electrodes and heavily doped Si back-gate (see Methods). At room temperature, the devices comprising as-made $w \approx 20$ nm GNR and GNR arrays typically showed I_{max}/I_{min} current ratios of less than ~3 (Supplementary Fig. S4)[5,6,8], indicating insufficient bandgap (compared to $k_BT \approx 26$ meV) for room-temperature FETs. The bandgap of a perfect GNR is predicted to scale inverse linearly with GNR widths, and $E_g \approx (0.3 - 1.5\ \text{eV nm})/w\ (\text{nm})$ depending on the orientation and edge configuration of the ribbons[12,13]. For GNRs narrowed down to ~10 nm, we observed an I_{max}/I_{min} ratio of ~10 at room temperature (Supplementary Fig. S5). Using long GNRs narrowed down to $w \approx 8$ nm with good continuity (Fig. 3b), we fabricated a FET comprising an array of GNRs arranged in parallel and with interdigitized electrodes as contacts (Fig. 4a). We observed a high I_{on}/I_{off} ratio of up to ~50 at room temperature, and an 'on' state current of ~20 μA (~40 times that of single-ribbon devices) at $V_{ds} = -500$ mV (Fig. 4b,c) with ~40 GNR sections (channel length ≈ 160 nm).

For GNRs narrowed down to the $w \lesssim 5$ nm regime, because of limitations resulting from discontinuity in the ribbons, we fabricated devices only on single ribbons rather than with parallel arrays. Figure 4e,f presents room-temperature $I_{ds} - V_{gs}$ and $I_{ds} - V_{ds}$ characteristics of a GNR-FET with a $w \approx 4$ nm GNR (see Supplementary Fig. S6 for another example). The device exhibited ambipolar transport in air with $I_{on}/I_{off} > 1 \times 10^4$ (Fig. 4e), clear evidence of bandgap opening through lateral quantum confinement[3–6,11–13]. This is the highest room-temperature I_{on}/I_{off} ratio reported for GNRs derived from lithographic patterning[6–9]. In vacuum, the device shows an intrinsic n-type behaviour, with the threshold voltage shifted to the negative gate voltage side due to desorption of physisorbed species including oxygen[23]. Based on ambipolar $I_{ds} - V_{gs}$ characteristics, we estimated the bandgap of the GNR to be $E_g \approx 0.4$ eV from $I_{on}/I_{off} \approx \exp(E_g/2k_BT)$, because the off-state current was thermally activated over a body-Schottky barrier of $\sim E_g/2$ (ref. 8).

In conclusion, we have developed a process for controlled chemical narrowing of graphene to yield quantum confined structures. Parallel GNR arrays were used to create graphene FETs with high 'on' currents and a high on/off ratio of ~50 at room temperature. Single ribbons based on lithography were narrowed to below ~5 nm to afford on/off ratios of $\sim 1 \times 10^4$. On the single-ribbon basis, our narrowed GNRs exhibited lower 'on' currents than our previously reported chemically derived sub-10-nm GNRs on the same 300-nm SiO_2 substrate[3]. The narrowed lithography-derived GNRs showed rougher and more disordered edges, as reflected from Raman spectroscopy data. Edge disorder caused scattering effects that contributed to the low 'on' currents of the GNR devices[4,24–26]. There were variations between the devices, such as doping, probably due to differences in the detailed edge structures. Clearly, the success of our approach is currently limited by the edge roughness introduced in the patterning process, and much

effort should be directed in the future towards making smooth edges by either improving the lithographic patterning processes or by developing novel chemical means to perfect the edges. Some recent experiments have demonstrated the promise of making graphene and GNRs with atomically well-defined edges by using anisotropic etching[27–30], which could be combined with narrowing to produce long, uniform sub-5-nm GNR semiconductors to produce high-performance graphene transistors for potential digital applications. This could lead to an appealing future for graphene, in particular because chemical narrowing of GNRs with well-defined crystallographic orientations could yield semiconducting GNRs with desired edge structures.

Methods

Preparation of mechanically exfoliated graphene, microscopy and spectroscopy characterizations, and lithographic patterning of GNRs. Graphene sheets used in etching experiments under various conditions were mechanically exfoliated from highly oriented pyrolitic graphite crystals on a thermally grown ~300-nm SiO_2/p^{++} Si substrate using Scotch tape[31]. Subsequent annealing in ~2 torr H_2 at 800 °C for ~15 min was carried out to clean the substrate and graphene sheets. AFM and Raman mapping were then used to characterize the graphene sheets before and after the gas-phase reaction. Raman mapping was carried out by a Horiba Jobin Yvon LabRAM HR Raman microscope with 633-nm He−Ne laser excitation (spot size, ~1 μm; power, ~5 mW). We used a step size of 100 nm and accumulation time of 4 s to map the graphene sheets.

The graphene sheets used for patterning the GNRs were mechanically exfoliated on a thermally grown ~300-nm SiO_2/p^{++} Si substrate with pre-patterned Ti/Au markers and were annealed at ~600 °C for ~15 min (Ti/Au markers melt at higher temperatures). We used an optical microscope to locate few-layer (≲3 layers) graphene sheets and then carried out Raman spectroscopy to determine the number of layers. We spun ~70-nm poly(methyl methacrylate) (PMMA) with a molecular weight of 950 kDa as the electron-beam lithography resist. Single pixel lines were exposed in a Raith 150 system in the Stanford Nanofabrication Facility with an acceleration voltage of 10 keV and line dosage of 650 μC cm^{-1}. Wider GNRs could be made by exposing areas instead of single pixel lines. Development was carried out in cold (4 °C) 1:3 methyl iso-butyl ketone:isopropanol solution for 75 s to provide a good edge roughness in the resist profile[32]. A 6.5-nm-thick Al film was then electron-beam evaporated, followed by standard liftoff. Argon plasma etching was carried out in an MRC plasma etcher for ~20–30 s (depending on the number of layers of graphene), under an Ar flow rate of ~10 cm^3 min^{-1}, chamber pressure of ~40 mtorr and plasma power of ~10 W. After plasma etching, the chips were soaked in 0.1 mol l^{-1} KOH water solution for ~2 min to remove the Al lines. We then annealed the chips in ~2 torr H_2 at 600 °C to clean resist any residues from the substrate.

Gas-phase chemical etching of graphene in a vacuum furnace. Gas-phase etching of the graphene sheets and narrowing of the GNRs were carried out in a vacuum furnace connected to a mechanical pump, with a base pressure of ~15 mtorr. Note that a leak-free vacuum system was essential to achieving high reproducibility in the etching results. From experience, we have found that the etching rate is sensitive to the detailed configuration of the vacuum furnace and may vary in different systems. The vacuum level in the furnace was monitored by a Millipore CML series 0−100 torr vacuum gauge. We used Praxair ultrahigh-purity grade Ar, H_2 and 10% NH_3 in Ar and research grade O_2 in our experiments. To adjust the pressure of the gases, we first closed all the gas valves and recorded the base pressure of the system. We then opened the valves, one gas at a time, and adjusted the pressure with manual valves. Once the pressure reached target and remained stable for ~1 min, we closed the valve and moved on to the next gas. Finally, we opened all the gas valves and began heating to reach the desired temperature. Because the pressure was adjusted manually, it is possible that there were some slight pressure variations for different batches, which could have led to slight variations in the etching rates.

Fabrication and electrical characterization of the GNR devices. After making (or narrowing) GNRs on the ~300-nm SiO_2/p^{++} Si substrate with pre-patterned Ti/Au markers, we used AFM to locate the GNR or GNR array relative to a marker. We then used electron-beam lithography to define the source and drain, followed by ~20-nm Pd evaporation and liftoff. The devices were annealed in Ar at ~200 °C to anneal the metal contacts. Electrical data of the GNR devices were taken using a standard semiconductor analyser (Agilent 4156C) inside a Lakeshore table-top cryogenic vacuum probe station connected to a turbo pump. The base pressure of the system was ~1×10^{-6} torr.

Received 10 December 2009; accepted 10 May 2010; published online 27 June 2010

References

1. Geim, A. K. & Novoselov, K. S. The rise of graphene. *Nature Mater.* **6,** 183–191 (2007).
2. Geim, A. K. Graphene: status and prospects. *Science* **324,** 1530–1534 (2009).
3. Li, X., Wang, X., Zhang, L., Lee, S. & Dai, H. Chemically derived, ultrasmooth graphene nanoribbon semidonductors. *Science* **319,** 1229–1232 (2008).
4. Wang, X. *et al.* Room-temperature all-semiconducting sub-10-nm graphene nanoribbon field-effect transistors. *Phys. Rev. Lett.* **100,** 206803 (2008).
5. Jiao, L., Zhang, L., Wang, X., Diankov, G. & Dai, H. Narrow graphene nanoribbons from carbon nanotubes. *Nature* **458,** 877–880 (2009).
6. Bai, J., Duan, X. & Huang, Y. Rational fabrication of graphene nanoribbons using a nanowire etching mask. *Nano Lett.* **9,** 2083–2087 (2009).
7. Han, M. Y., Ozyilmaz, B., Zhang, Y. & Kim, P. Energy bandgap engineering of graphene nanoribbons. *Phys. Rev. Lett.* **98,** 206805 (2007).
8. Chen, Z., Lin, Y.-M., Rooks, M. J. & Avouris, P. Graphene nano-ribbon electronics. *Physica E* **40,** 228–232 (2007).
9. Pomomarenko, L. A. *et al.* Chaotic Dirac billiard in graphene quantum dots. *Science* **320,** 356–358 (2008).
10. Kosynkin, D. V. *et al.* Longitudinal unzipping of carbon nanotubes to form graphene nanoribbons. *Nature* **458,** 872–876 (2009).
11. Nakada, K., Fujita, M., Dresselhaus, G. & Dresselhaus, M. S. Edge state in graphene ribbons: nanometer size effect and edge shape dependence. *Phys. Rev. B* **54,** 017954–017961 (1996).
12. Son, Y.-W., Cohen, M. L. & Louie, S. G. Energy gaps in graphene nanoribbons. *Phys. Rev. Lett.* **97,** 216803 (2006).
13. Barone, V., Hod, O. & Scuseria, G. E. Electronic structure and stability of semiconducting graphene nanoribbons. *Nano Lett.* **6,** 2748–2754 (2006).
14. Wang, X., Tabakman, S. M. & Dai, H. Atomic layer deposition of metal oxides on pristine and functionalized graphene. *J. Am. Chem. Soc.* **130,** 8152–8153 (2008).
15. Lee, S. M., Lee, Y. H., Hwang, Y. G., Hahn, J. R. & Kang, H. Defected-induced oxidation of graphite. *Phys. Rev. Lett.* **82,** 217–220 (1999).
16. Hahn, J. R., Kang, H., Lee, S. M. & Lee, Y. H. Mechanistic study of defect-induced oxidation of graphite. *J. Phys. Chem. B* **103,** 9944–9951 (1999).
17. Ni, Z. H. *et al.* Uniaxial strain on graphene: Raman spectroscopy study and bandgap opening. *ACS Nano* **2,** 2301–2305 (2008).
18. Mohiuddin, T. M. G. *et al.* Uniaxial strain in graphene by Raman spectroscopy: G peak splitting, Gruneisen parameters and sample orientation. *Phys. Rev. B* **79,** 205433 (2009).
19. Li, X. *et al.* Simultaneous nitrogen-doping and reduction of graphene oxide. *J. Am. Chem. Soc.* **131,** 15939–15944 (2009).
20. Yan, Q. *et al.* Intrinsic current−voltage characteristics of graphene nanoribbon transistors and effect of edge doping. *Nano Lett.* **7,** 1469–1473 (2007).
21. OuYang, F., Xiao, J., Guo, R., Zhang, H. & Xu, H. Transport properties of T-shaped and cross junctions based on graphene nanoribbons. *Nanotechnology* **20,** 055202 (2009).
22. Ferrari, A. C. Raman spectroscopy of graphene and graphite: disorder, electron-phonon coupling, doping and nonadiabatic effects. *Solid State Commun.* **143,** 47–57 (2007).
23. Wang, X. *et al.* N-doping of graphene through electrothermal reactions with ammonia. *Science* **324,** 768–771 (2009).
24. Zhao, P., Choudhury, M., Mohanram, K. & Guo, J. Computational model of edge effects in graphene nanoribbon transistors. *Nano Res.* **1**, 395–402 (2008).
25. Yoon, Y. & Guo, J. Effect of edge roughness in graphene nanoribbon transistors. *Appl. Phys. Lett.* **91,** 073103 (2007).
26. Cresti, A. *et al.* Charge transport in disordered graphene-based low dimensional materials. *Nano Res.* **1,** 361–394 (2008).
27. Ci, L. *et al.* Controlled nanocutting of graphene. *Nano Res.* **1,** 116–122 (2008).
28. Campos, L. C., Manfrinato, V. R., Sanchez-Yamagishi, J. D., Kong, J. & Jarillo-Herrero, P. Anisotropic etching and nanoribbon formation in single-layer graphene. *Nano Lett.* **9,** 2600–2604 (2009).
29. Datta, S. S., Strachan, D. R., Khamis, S. M. & Johnson, A. T. C. Crystallographic etching of few-layer graphene. *Nano Lett.* **8,** 1912–1915 (2008).
30. Nemes-Incze, P., Magda, G., Kamaras, K. & Biro, L. P. Crystallographically selective nanopatterning of graphene on SiO_2. *Nano Res.* **3,** 110–116 (2010).
31. Novoselov, K. S. *et al.* Electric field effect in atomically thin carbon films. *Science* **306,** 666–669 (2004).
32. Hu, W., Sarveswaran, K., Lieberman, M. & Bernstein, G. H. Sub-10-nm electron beam lithography using cold development of poly(methylmethacrylate). *J. Vac. Sci. Technol. B* **22,** 1711–1716 (2004).

Acknowledgements

This work was supported by Intel, the MARCO MSD Center and Graphene MURI (the Office of Naval Research). The authors are grateful to J.W. Conway from the Stanford Nanofabrication Facility for helpful discussions.

Author contributions

X.W. and H.D. conceived and designed the experiments. X.W. performed the experiments and analysed the data. X.W. and H.D. co-wrote the paper. Both authors discussed the results and commented on the manuscript.

Additional information

The authors declare no competing financial interests. Supplementary information accompanies this paper at www.nature.com/naturechemistry. Reprints and permission information is available online at http://npg.nature.com/reprintsandpermissions/. Correspondence and requests for materials should be addressed to H.D.